J|A|C|S ARTICLES

Published on Web 02/15/2010

Three-Level Topology Switching in a Molecular Möbius Band

Marcin Stępień,* Bartosz Szyszko, and Lechosław Latos-Grażyński*

Wydział Chemii, Uniwersytet Wrocławski, ul. F. Joliot-Curie 14, 50-383 Wrocław, Poland

Received November 23, 2009; E-mail: ms@wchuwr.pl; llg@wchuwr.pl

Ⓦ **This paper contains enhanced objects available on the Internet at http://pubs.acs.org/jacs.**

Abstract: Möbius π-conjugation in cyclic molecules leads to the reversal of Hückel aromaticity rules and affects the electronic and magnetic properties of these systems. We found the first example of a medium-sized macrocyclic structure that is sufficiently flexible to switch between three distinct π-conjugation topologies, planar (**T0**), Möbius (**T1**), and twisted Hückel (**T2**), without changing its oxidation level. The switching is under thermodynamic and kinetic control and can be realized in a three- or four-step cycle. On titration with trifluoroacetic acid (TFAH) or dichloroacetic acid (DCAH), the Möbius free base (**T1**-H_2), which is the preferred structure in dichlorofluoromethane at 150 K, undergoes a series of acid−base reactions involving changes of the π-conjugation topology. The forms observed in the course of titration involve a Möbius aromatic monocation ([**T1**-H_3]$^+$), an antiaromatic twisted Hückel species ([**T2**-H_4(A)]$^+$) containing a coordinated carboxylate anion (A = TFA, DCA), and two additional Möbius forms ([**T1**-H_4(A)(HA)$_n$]$^+$ (n = 1, 2)), containing complex carboxylate anions. The protonated forms undergo a thermally activated ring planarization to yield an antiaromatic quasi-planar dication [**T0**-H_4]$^{2+}$, characterized in the solid state as a TFA salt. The corresponding free base (**T0**-H_2) is metastable but can be trapped by addition of triethylamine at low temperatures.

Introduction

π-Conjugated systems in the form of a Möbius strip were first discussed by Heilbronner in 1964, who predicted that Hückel's aromaticity rules would be reversed for π-surfaces with an odd number of half-twists.[1] However, the structural requirements imposed by Möbius π-conjugation are not easily fulfilled, and the first example of a stable, neutral Möbius aromatic molecule was only revealed almost 40 years later.[2−4] Möbius strip conformations were subsequently identified in a number of expanded porphyrins,[5] in which they are commonly stabilized by steric hindrance resulting from peripheral substitution or by metal coordination.[6−14] It was shown that topologies with a single half-twist can be induced in macrocyclic rings consisting of three to eight cyclic subunits[7,8] and that, in the case of larger rings, Möbius π-conjugation leads to appreciable diatropic ring currents observable by ^{1}H NMR spectroscopy.[8] In spite of these advances, Möbius aromaticity remains a rare phenomenon and no easily applicable method has been proposed of constructing π-surfaces with a stable 180° twist.

An interesting feature of Möbius aromatics, which distinguishes them from a Möbius band made of paper, is their ability to change the degree of twist without dissecting the ring. Such a change of topology is achieved via internal rotations and, if properly controlled, can provide access to molecular switches with unique optical and magnetic properties.[15] However, as the formation of a Möbius π-surface was usually the primary objective, the majority of systems studied to date were made deliberately rigid to avoid their irreversible conversion to a potentially more stable Hückel-type form.[2,8,10,12] Nevertheless, in a few instances, reversible switching was observed between a Möbius structure and either a doubly twisted[6,9,16] or planar conformation.[7,11,13] The prototypical example of such a switch was A,D-di-*p*-benzihexaphyrin (Figure 1), in which two rotating *p*-phenylene rings act as "topology selectors".[6] The macrocycle

(1) Heilbronner, E. *Tetrahedron Lett.* **1964**, *5*, 1923–1928.
(2) Ajami, D.; Oeckler, O.; Simon, A.; Herges, R. *Nature* **2003**, *426*, 819–821.
(3) Ajami, D.; Hess, K.; Köhler, F.; Näther, C.; Oeckler, O.; Simon, A.; Yamamoto, C.; Okamoto, Y.; Herges, R. *Chem. Eur. J.* **2006**, *12*, 5434–5445.
(4) Herges, R. *Chem. Rev.* **2006**, *106*, 4820–4842.
(5) Sessler, J. L.; Seidel, D. *Angew. Chem., Int. Ed.* **2003**, *42*, 5134–5175.
(6) Stępień, M.; Latos-Grażyński, L.; Sprutta, N.; Chwalisz, P.; Szterenberg, L. *Angew. Chem., Int. Ed.* **2007**, *46*, 7869–7873.
(7) Pacholska-Dudziak, E.; Skonieczny, J.; Pawlicki, M.; Szterenberg, L.; Ciunik, Z.; Latos-Grażyński, L. *J. Am. Chem. Soc.* **2008**, *130*, 6182–6195.
(8) Tanaka, Y.; Saito, S.; Mori, S.; Aratani, N.; Shinokubo, H.; Shibata, N.; Higuchi, Y.; Yoon, Z. S.; Kim, K. S.; Noh, S. B.; Park, J. K.; Kim, D.; Osuka, A. *Angew. Chem., Int. Ed.* **2008**, *47*, 681–684.
(9) Saito, S.; Shin, J.-Y.; Lim, J. M.; Kim, K. S.; Kim, D.; Osuka, A. *Angew. Chem., Int. Ed.* **2008**, *47*, 9657–9660.
(10) Park, J. K.; Yoon, Z. S.; Yoon, M.-C.; Kim, K. S.; Mori, S.; Shin, J.-Y.; Osuka, A.; Kim, D. *J. Am. Chem. Soc.* **2008**, *130*, 1824–1825.
(11) Sankar, J.; Mori, S.; Saito, S.; Rath, H.; Suzuki, M.; Inokuma, Y.; Shinokubo, H.; Suk Kim, K.; Yoon, Z. S.; Shin, J.-Y.; Lim, J. M.; Matsuzaki, Y.; Matsushita, O.; Muranaka, A.; Kobayashi, N.; Kim, D. H.; Osuka, A. *J. Am. Chem. Soc.* **2008**, *130*, 13568–13579.
(12) Tokuji, S.; Shin, J.-Y.; Kim, K. S.; Lim, J. M.; Youfu, K.; Saito, S.; Kim, D.; Osuka, A. *J. Am. Chem. Soc.* **2009**, *131*, 7240–7241.
(13) Kim, K. S.; Yoon, Z. S.; Ricks, A. B.; Shin, J.-Y.; Mori, S.; Sankar, J.; Saito, S.; Jung, Y. M.; Wasielewski, M. R.; Osuka, A.; Kim, D. *J. Phys. Chem. A* **2009**, *113*, 4498–4506.
(14) Yoon, Z. S.; Osuka, A.; Kim, D. *Nature Chem.* **2009**, *1*, 113–122.
(15) Feringa, B. *Molecular Switches*.; Wiley-VCH: Weinheim, Germany, 2001;.
(16) Koide, T.; Youfu, K.; Saito, S.; Osuka, A. *Chem. Commun.* **2009**, 6047–6049.

10.1021/ja909913y

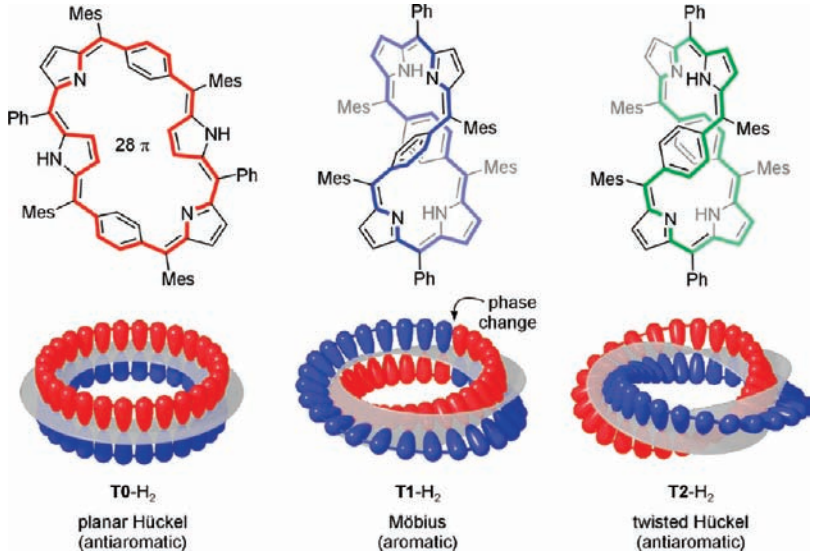

Figure 1. Three topologies of the π-conjugated surface available for A,D-di-*p*-benzihexaphyrin. **T0**, **T1**, and **T2**, labeled according to the number of half-twists, denoting respectively the planar Hückel, Möbius, and twisted (figure-eight) Hückel topologies. The Hückel structures are both double-sided, but in the twisted form the two lobes of the π-cloud are interlocked. The protonation status of the macrocycle will be denoted with an appropriate suffix (e.g., **T1**-H_2). Protonation patterns of the free bases **T0**-H_2 and **T1**-H_2 have been observed experimentally, whereas the tautomer of **T2**-H_2 shown in the figure was selected on the basis of DFT calculations.

is folded into a figure-eight structure and, depending on the relative orientation of the phenylene rings, it adopts a conformation with either one or two half-twists (**T1**-H_2 and **T2**-H_2, respectively). Because of the [4*n*]annulenoid pathway present in the macrocycle, the conformer **T1**-H_2 is an aromatic Möbius system, whereas the double-sided structure **T2**-H_2 exhibits the more typical Hückel antiaromaticity. Here we show that A,D-di-*p*-benzihexaphyrin can act as a tristable aromaticity switch with three π-surface topologies: planar (**T0**), singly twisted (**T1**), and doubly twisted (**T2**), all of which are accessible at a single oxidation level of the macrocycle. This extension of switching range is achieved by combining thermodynamic and kinetic control and enables the simultaneous observation of three types of π-conjugation in a single system. Additionally, even though some switching steps are irreversible, it is possible to perform them in a closed cycle. The degree of structural control observed in di-*p*-benzihexaphyrin offers a paradigm for creating molecular switches with more than two accessible states. Such molecules, which can be stimulated by light, pH, or cation binding,[17] have been considered as precursors to such molecular electronics devices as logic gates[18] or high-density data storage.[19] A variety of multistate switches relying on tunable π-delocalization have been proposed, but to date, they are limited to various planar Hückel motifs.[17,19−22] The system proposed herein combines mechanical and π-electron switching, providing a potentially versatile route to molecular devices.

Results and Discussion

Overview of the Switching Process. When it is dissolved in dichlorofluoromethane-*d* (DCFM-*d*) at 150 K, A,D-di-*p*-benzihexaphyrin exists exclusively as the Möbius conformer **T1**-H_2. During titrations with trifluoroacetic acid (TFAH) or dichloroacetic acid (DCAH) **T1**-H_2 undergoes a two-step protonation followed by association of acid molecules (Figure 2A). The sequences of events, illustrated by the speciation graph for the DCAH titration (Figure 2B), are qualitatively similar for both acids. In the initial phase of the titration, **T1**-H_2 is converted to the monocation [**T1**-H_3]$^+$, which is structurally similar to the free base and retains the Möbius π-surface. The second protonation step, closely overlapping with the first one, is combined with a well-defined anion binding event and leads to a new antiaromatic species, [**T2**-H_4(A)]$^+$ (A = TFA, DCA), in which the π-surface topology has switched to the twisted Hückel form. This topology change, which results from an internal rotation of one of the phenylene rings, is necessary to accommodate the carboxylate anion in the macrocyclic core. The carboxylic group of the anion is hydrogen-bonded to the four NH groups in the core, whereas the substituted methyl group (R = CF_3, $CHCl_2$) is confined in one of the two grooves formed by the figure-eight **T2** conformation (Figure 3).

In the second switching step, induced by further titration at 150 K, the anion bound to the twisted Hückel form [**T2**-H_4(A)]$^+$ is partially released from the macrocyclic core to react with an additional acid molecule. In the species that forms, [**T1**-H_4(A)(HA)]$^+$, the macrocycle is restored to the Möbius conformation, and the resulting structure contains a hydrogen bis(carboxylate) anion, which is held in one of the grooves by two hydrogen bonds (Figure 3). At higher acid concentrations, [**T1**-H_4(A)(HA)]$^+$ converts to a structurally related system, [**T1**-H_4(A)(HA)$_2$]$^+$, containing three acid units, which is the ultimate species observed during the titration. The additional acid

(17) Maestri, M.; Pina, F.; Balzani, V., Multistate/Multifunctional Molecular-Level Systems - Photochromic Flavylium Compounds. In *Molecular Switches*; Feringa, L. B., Ed.; Wiley-VCH: Weinheim, Germany, 2001; p 339.
(18) Brown, G. J.; De Silva, A. P.; Pagliari, A. *Chem. Commun.* **2002**, 2461–2464.
(19) Irie, M. *Chem. Rev.* **2000**, *100*, 1685–1716.
(20) Frigoli, M.; Mehl, G. H. *Angew. Chem., Int. Ed.* **2005**, *44*, 5048–5052.
(21) Niemz, A.; Rotello, V. M. *Acc. Chem. Res.* **1999**, *32*, 44–52.
(22) Mitchell, R. H.; Bohne, C.; Wang, Y.; Bandyopadhyay, S.; Wozniak, C. B. *J. Org. Chem.* **2006**, *71*, 327–336.

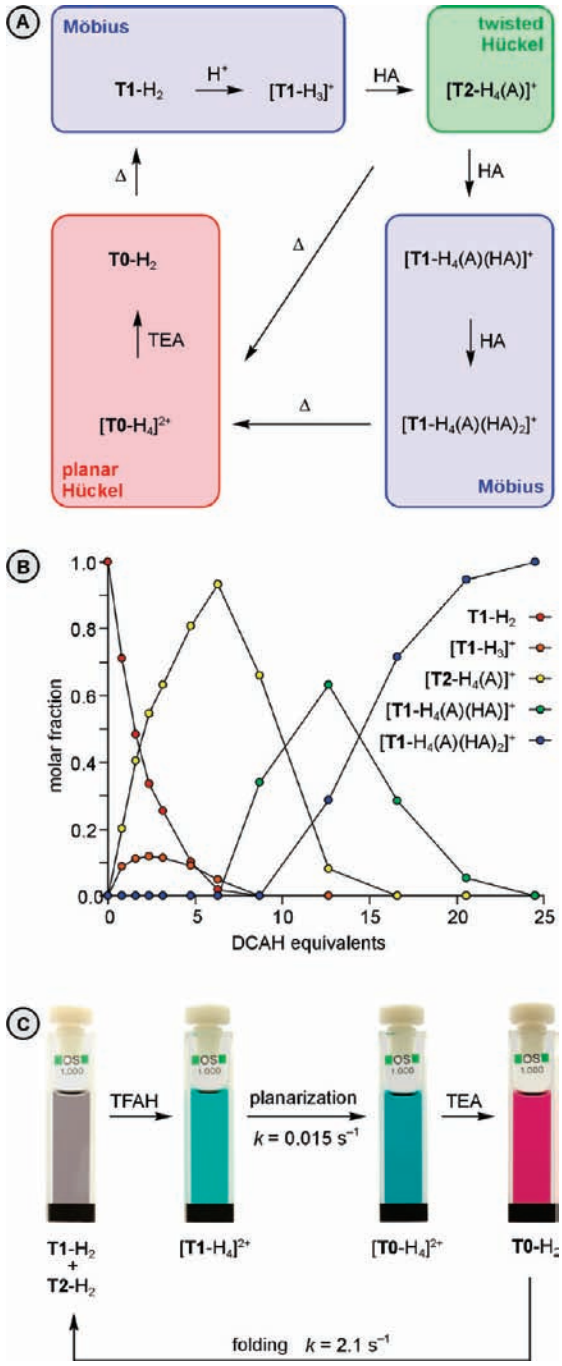

Figure 2. (A) Switching between the three different π-conjugation topologies of A,D-di-*p*-benzihexaphyrin performed in DCFM-*d* solution at 150 K. The reversibility of some processes is not indicated. For each species, its abbreviated formula indicates the π-conjugation topology, protonation status, associated anions and acid molecules, and total charge. Additional symbols used: HA, acid (TFAH or DCAH); TEA, triethylamine; Δ, heating to 270 K to induce conversion, then cooling back to 150 K. (B) Distribution curves for the titration of **T1**-H_2 with dichloroacetic acid (150 K, DCFM-*d*). Data points were obtained by deconvolution of ^{1}H NMR spectra. Lines are for illustration only. (C) Color changes caused by the planarization of the dication and subsequent folding of the free base (DCM, 298 K). WEO1, available on the Web version of the article, contains a movie showing the color changes depicted in Figure 2C.

molecule is loosely bound to one end of the hydrogen bis(carboxylate) anion (Figure 3). The ability of carboxylic acids to form hydrogen-bonded complexes with their conjugate bases is a known phenomenon, and species characterized as A(HA) and (AH)A(HA) were identified in solution using low-temperature NMR spectroscopy.[23]

[**T2**-H_4(A)]$^+$ and subsequent cationic forms described above are metastable and undergo spontaneous conversion to the quasiplanar antiaromatic structure [**T0**-H_4]$^{2+}$ at temperatures above 190 K. This process, which constitutes another topology switching step, can be conveniently studied at room temperature by means of UV−vis spectroscopy (Figure 2C). Initially, the free base, which forms an equilibrium mixture of **T1**-H_2 and **T2**-H_2 when dissolved in dichloromethane (DCM),[6] is converted to the [**T1**-H_4]$^{2+}$ dication by addition of 2 equiv or more of TFAH. The turquoise Möbius species begins to transform into [**T0**-H_4]$^{2+}$ immediately after the addition of acid, with a subtle color change to a more bluish (cerulean) hue. The reaction is a first-order process with a rate constant of 0.015 s^{-1} at 298 K and shows no significant dependence on the concentration of acid (2 vs 10 equiv) or its identity (TFAH vs DCAH). As seen in the X-ray structure of a TFA salt (Figure 3), the **T0** dication contains two inverted pyrrole rings,[24] a structural feature that partially relieves the strain due to planarization.

When a solution of [**T0**-H_4]$^{2+}$ is treated with triethylamine, the dication is converted to the corresponding free base, **T0**-H_2, which retains the planar Hückel topology of its π-surface. **T0**-H_2 is distinguished from the other two conformers by its ruby color (**T1**-H_2 and **T2**-H_2 are respectively violet and green). At room temperature in DCM solution, the **T0**-H_2 free base is unstable and quantitatively converts to the equilibrium mixture of **T1**-H_2 and **T2**-H_2 within just a few seconds. With a rate constant of 2.1 s^{-1} at 298 K, the folding transformation is significantly faster than the planarization process observed for cations, the latter taking several hours to complete at the same temperature. This last transformation completes the switching cycle depicted in Figure 2. As [**T0**-H_4]$^{2+}$ can be directly obtained from both [**T2**-H_4(A)]$^+$ and [**T1**-H_4(A)$(HA)_2$]$^+$, the cycle can be closed in either three or four steps, depending on the amount of added acid.

Solution Structures. The mechanism of aromaticity switching, summarized in Figure 2A, was elucidated by extensive application of proton magnetic resonance spectroscopy (^{1}H NMR) in combination with electronic spectroscopy, X-ray diffraction measurements, and high-level DFT calculations. The analysis of proton magnetic resonance data presented in this work relied on extensive use of variable-temperature experiments and homonuclear correlation spectroscopy. Given the complicated nature of investigated dynamic processes, no quantitative line shape analysis was attempted. Information on scalar couplings was obtained from gradient-selected COSY spectra. Dipolar couplings and chemical exchange patterns were identified by parallel use of NOESY and ROESY experiments and careful comparison of results obtained from these two techniques. Under the usual experimental conditions (DCM-d_2 or DCFM-*d* solvents, temperatures below 190 K, 600 MHz base frequency), the observed NOE's corresponded to the slow-motion limit, providing excellent sensitivity in the NOESY maps. On the other hand, the NOE's were of the same sign as the EXSY correlations, and the two processes could only be discerned from each other with the aid of ROESY spectra. When precise information on dipolar couplings was sought, the experiment temperature

(23) Tolstoy, P. M.; Schah-Mohammedi, P.; Smirnov, S. N.; Golubev, N. S.; Denisov, G. S.; Limbach, H.-H. *J. Am. Chem. Soc.* **2004**, *126*, 5621–5634.
(24) Furuta, H.; Maeda, H.; Osuka, A. *Chem. Commun.* **2002**, 1795–1804.

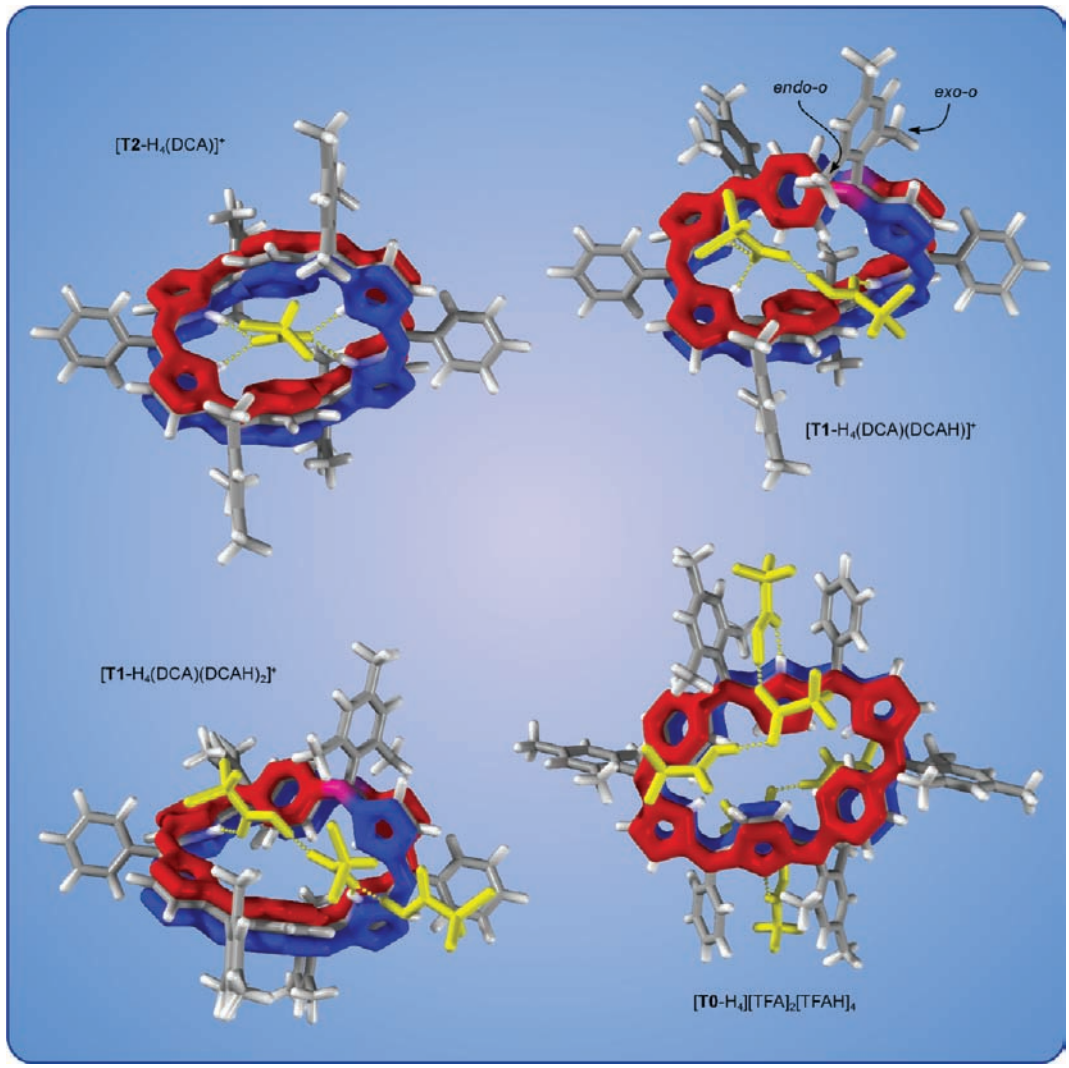

Figure 3. DFT-optimized geometries (B3LYP/6-31G**) of [**T2**-H_4(DCA)]$^+$, [**T1**-H_4(DCA)(DCAH)]$^+$, and [**T1**-H_4(DCA)(DCAH)$_2$]$^+$ and an X-ray diffraction structure of [**T0**-H_4][TFA]$_2$[TFAH]$_4$. The topology of the π-conjugation surface is shown schematically in red and blue, with the phase change in **T1** systems highlighted in purple. DCA and TFA residues and hydrogen bonding are shown in yellow.

was chosen so that any exchange was too slow to interfere with NOE patterns. Chemical shift values are given in Table S4.

Symmetry Considerations and Labeling Convention. The numbering scheme of the hexaphyrin ring, used in previous work,[6,25] is shown in Figure 4A. In the present discussion we will employ a different labeling convention, which facilitates comparison between different structures and fully exploits the symmetry of the macrocycle. The structure is formally dissected across phenylene rings and phenyl-substituted meso bridges, as shown in Figure 4B. Each of the resulting quadrants contains one pyrrole ring, a half of a phenylene ring, and one mesityl substituent. Phenyl substituents are not included in the analysis because the corresponding signals were normally difficult to identify unambiguously and consequently had little use in the assignment process. In the text, the quadrants will be denoted with bold letters (**a**−**d**). Depending on the effective molecular symmetry, the quadrants may show complete nonequivalence (C_1 symmetry), pairwise equivalence (2-fold symmetries), or complete equivalence (higher symmetries, Figure 4C). For figure-eight **T1** and **T2** conformers, the nonequivalent positions within each quadrant are labeled as shown in Figure 4D. By default, *in*-phenylene corresponds to the position proximal to the nitrogen, whereas *endo-o*-Mes is the methyl group closer to the *z* axis. It should be noted that adjacency of *in* and *out* positions within each phenylene ring depends on its relative orientation within the macrocyclic framework. If the normal of the phenylene ring is parallel to the *z* axis (as in one ring of the **T1** conformer), the *in* position is adjacent to the *in* position of the adjoining quadrant. If the phenylene normal is perpendicular to the *z* axis (as in both rings of the **T2** conformer), the *in* position is adjacent to an *out* position. In the case of the **T0** conformer, differentiation between *in*- and *out*-phenylene positions is straightforward; however, for practical reasons, no distinction is made between the nonequivalent ortho and meta positions on the aryl substituents.

Depending on the particular species and the rate of pertinent dynamic processes at a given temperature, the observed spectral patterns correspond to various effective symmetries. The relevant symmetries available for the hexaphyrin framework are summarized in Table S3, which includes supergroup−subgroup relationships and expected signal multiplicities (for axis labeling see Figure 4B). The Schoenflies symbols are used throughout

(25) Stępień, M.; Szyszko, B.; Latos-Grażyński, L. *Org. Lett.* **2009**, *11*, 3930–3933.

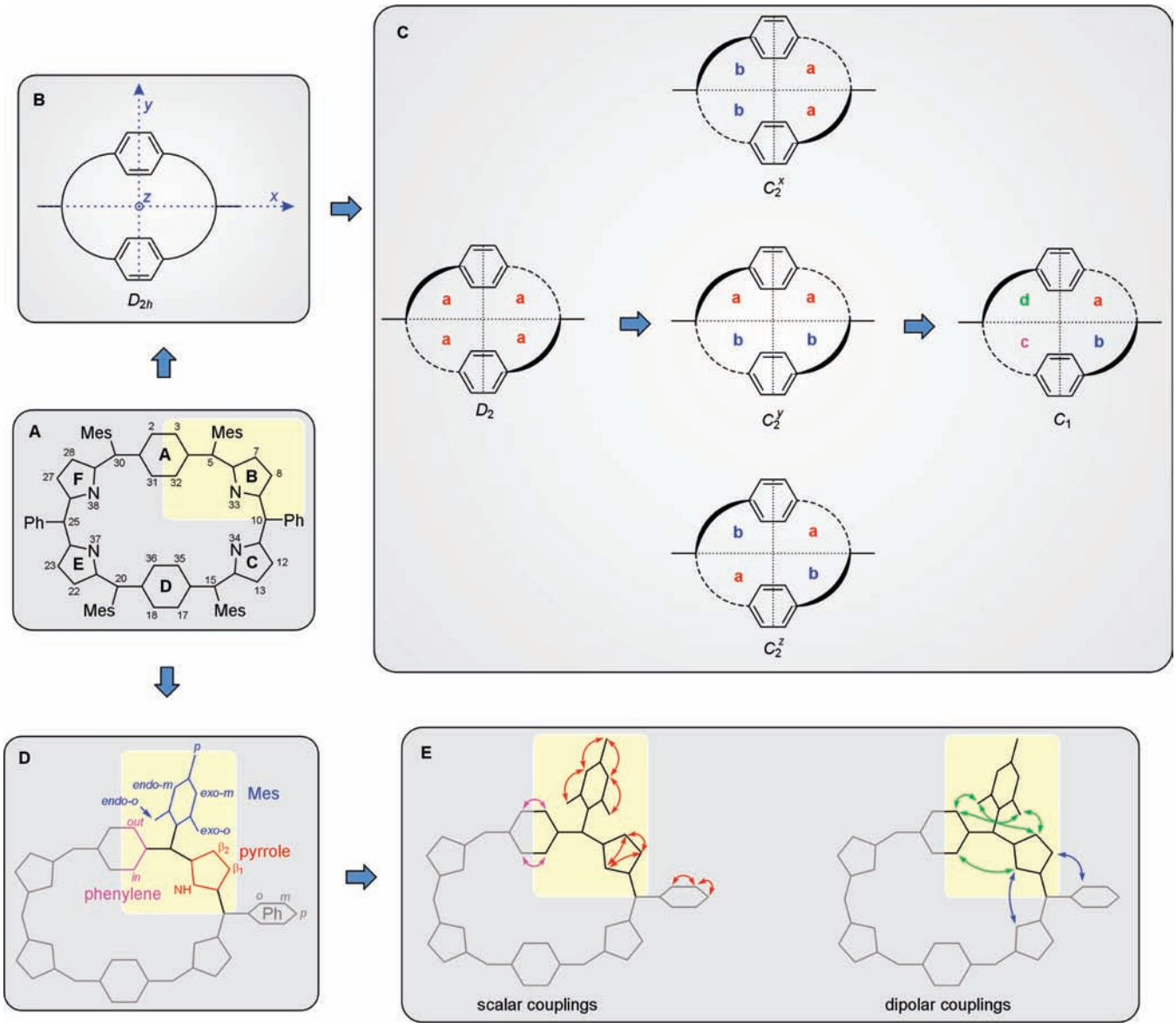

Figure 4. (A) Conventional numbering scheme for A,D-di-*p*-benzihexaphyrin.[6] One of the four equivalent quadrants is highlighted. (B) Hypothetical planarized conformation of the macrocycle, exhibiting D_{2h} symmetry and the definition of molecular axes. (C) Symmetry lowering in figure-eight conformers (**T1** and **T2**) and equivalence relationships between quadrants. (D) Quadrant labeling scheme (hydrogens are implicit). For definitions of *exo*/*endo* and *in*/*out* positions see text. (E) Correlations used in the initial stage of the assignment. Intra- and interquadrant scalar couplings observable by COSY are shown as red and purple arrows, respectively. "Trivial" dipolar couplings observable by NOESY/ROESY are shown as green and blue arrows corresponding to intra- and interquadrant contacts, respectively. For a detailed discussion of the figure see text.

the discussion, but they denote equivalence classes of observed signals rather than geometrical point symmetries. The equivalence classes may reflect (a) signal multiplicites observed directly in one-dimensional spectra and (b) exchange patterns observed via NOESY/ROESY. The Schoenflies symbols are further extended with the subscript *r*, which denotes freely rotating phenylene rings and complete *in*−*out* equivalence of phenylene signals.

Analysis of NMR Spectra. The assignment process was a relatively simple task in the case of the quasi-planar **T0** conformer. The analysis was significantly more complicated in the case of low-symmeric **T1** and **T2** structures, for which it was carried out in a number of stages.

1. Identification of Spin Systems using COSY Maps. The relevant correlations that could be identified include both ^3J and ^4J couplings, as shown in Figure 4E. Except for the ^3J couplings within the phenylene rings, the scalar correlations did not provide any information on interquadrant connectivity. The observation of four-bond couplings, while not always possible, was of special value as it was instrumental in the identification of NH signals. Occasionally, a careful choice of the measurement temperature was necessary to observe ^4J couplings. In the case of the free base **T1**-H_2, a crucial correlation between NH-**b** and β_2-**b** could only be detected at 140 K and was not observable at either 130 or 150 K.

2. Identification of Intraquadrant ("Trivial") NOE Contacts. This helped establish spatial relationships between the nonequivalent positions within each quadrant (Figure 4E).

3. Identification of "Nontrivial" NOE Contacts. These crucial NOE's were observed: (a) within phenylene rings; (b) between adjacent NH protons (i.e., within each dipyrromethene subunit); (c) occasionally between *endo*-*o*-Mes groups across the mac-

rocyclic ring; (d) between the protons of coordinated anions or acid molecules (O*H* for TFA and DCA, C*H*Cl_2 for DCA) and the proximate protons in the macrocycle. These last signals were a direct proof of structurally well-defined interactions between the hexaphyrin molecule and acid residues.

4. Analysis of Exchange Patterns. Intramolecular exchange was used whenever possible to validate the integrity of the assignment obtained from COSY and NOE data. The experiment temperature was chosen so as to optimize EXSY cross-peak intensity, while retaining possibly narrow linewidths. Intermolecular exchange could be observed in some instances, providing an additional test for the proposed assignments. Dynamic processes observed in solution are summarized in Figures 5−11.

5. Analysis of Macrocyclic Ring Currents. Aromatic molecules exhibit downfield shifts of protons attached to the periphery of the π-conjugated rings, whereas protons located inside the ring, if present, give rise to resonances that are shifted markedly upfield, often into the negative region of the δ scale.[26] For antiaromatic systems, this so-called ring current is reversed: i.e., the inner protons are deshielded and the outer ones experience a shielding effect. These two different ring currents are termed diatropic and paratropic,[27] respectively, and provide a means of differentiating between aromatic and antiaromatic strucures. Ring currents of moderate intensity were previously observed in the Möbius species **T1**-H_2 (diatropic) and the Hückel species **T2**-H_2 (paratropic).[6] In the present analysis, once the signal assignment was complete, the ring currents provided immediate information on the topology of the conformer under study (**T0** or **T2** vs **T1**).

6. Chemical Shift Prediction Using the GIAO Method. The shifts calculated at the KMLYP/6-31G(d,p) level of theory are in very good agreement with those obtained experimentally for the free bases. The predicted shifts are less accurate for charged species, but they nevertheless provide a quantitative picture consistent with experimental findings. The largest discrepancies are observed for the internal protons of the macrocycle, whose shifts are extremely sensitive to subtle variations of geometry (see Figures S9−15 for correlation plots).

Signal assignments and, consequently, the corresponding three-dimensional structures were derived from correlation spectra. It should be noted, however, that occasionally certain cross-peaks were difficult or impossible to locate in the 2D maps. Such problems were caused by (a) significant overlap of signals in certain areas, (b) inherently low cross-peak intensity, as in the case of ^4J couplings, and (c) very small chemical shift differences between correlating signals. However, the correlation data potentially available for each system are redundant, and the spectra could be interpreted for the majority of species discussed, even when some correlations were missing. The two exceptions were [**T1**-H_3]$^+$ and [**T1**-H_4(A)(HA)]$^+$, each of which is always accompanied by other species, for all studied conditions. For these two systems, severe crowding of 2D spectra allowed only partial assignment; however, this was sufficient to confirm their identity.

In the early stages of low-temperature NMR titrations, the hydrogen dicarboxylate anion [AHA]$^-$ (A = TFA, DCA), was consistently observed as a discrete species in solution. The O*H*···O proton of this anion (DCFM-*d*, 150 K) gives a very sharp signal at 19.99 ppm (A = TFA) or 19.67 ppm (A = DCA), and the $CHCl_2$ shift is 5.99 ppm for A = DCA. At higher acid concentrations these signals gradually shifted and increased in line width.

T1-H_2. As discussed in earlier work,[6] rotation of phenylene rings is very rapid in the free base (Figure 5), and the slow exchange limit could not be reached under typical conditions (variable-temperature measurements in chloroform-*d* or dichloromethane-d_2). In DCFM-*d*, the slow exchange limit is reached at 150 K, but full suppression of exchange correlations in NOESY and ROESY spectra is only achieved at 130 K. The ^{1}H NMR spectrum obtained in DCFM-*d* (Figure S2) has an effective $C_2{}^y$ symmetry and is fully consistent with a moderately diatropic figure-eight structure with Möbius topology. Only one tautomer is observed at low temperatures, with both NH protons located in the **b** quadrants (**bb**-H_2; see Figure 4 for labeling of quadrants). Somewhat surprisingly, the preferred solution tautomer is different from that present in the reported X-ray structure of **T1**-H_2,[6] in which the NH protons reside in the **a** quadrants (**aa**-H_2). In the gas-phase calculations (B3LYP/6-31G**), the **aa**-H_2 tautomer is predicted to be more stable than **bb**-H_2 by ca. 2 kcal/mol (Table S5); thus, the actual energy ordering may be easily affected by solvation or crystal-packing forces. The chemical shifts of the solution tautomer **bb**-H_2 are accurately reproduced by a GIAO calculation performed at the KMLYP/6-31G** level (Figure S9). A very accurate fit is also obtained between the fast-exchange data for **T2**-H_2[6] and averaged GIAO/KMLYP shifts, confirming the general applicability of this computational approach (Figure S10).

[T1-H_3]$^+$. The monocationic form [**T1**-H_3]$^+$ is observed in the early stage of titration (Figure S6) and is always accompanied by larger amounts of either the free base, **T1**-H_2, or the subsequent species, [**T2**-H_4(A)]$^+$ (the molar fraction of [**T1**-H_3]$^+$ never exceeds 0.15). As a consequence, the one-dimensional ^{1}H NMR spectra are very crowded and their complete analysis was not feasible. Nevertheless, several resonances of [**T1**-H_3]$^+$, including the NH peaks, were identified and assigned, providing sufficient proof for the identity of this species (Figure S2). Two tautomers are possible for [**T1**-H_3]$^+$, both of which are characterized by C_1 symmetry in the absence of exchange. The tautomer actually present in solution has the protonation pattern **bcd**-H_3 and was identified on the basis of relative cross-peak intensities in the ROESY spectrum (Figure 6) and the correlation between experimental and calculated shifts (Figure S10). The calculated shifts correlate reasonably well with the experimental values, the one exception being the shift of NH-**d**, which is predicted to appear at field higher than actually observed. This discrepancy is most likely a result of weak hydrogen bonding with the DCA anion, which causes a downfield relocation of the signal. The NH proton residing in the singly protonated dipyrromethene unit of the macrocycle moves between the two neighboring nitrogens (quadrants **a** and **b**), producing a distinct exchange pattern at 170 K (Figures 5 and 6). This exchange pattern suggests that the rotation of phenylenes is restricted and coupled to the transfer of the NH protons (see Figure 6 for details).

[T2-H_4(A)]$^+$. The paratropic structure [**T2**-H_4(A)]$^+$ is observed during the titration with both TFAH and DCAH (Figures 7 and S6). The spectrum obtained in the presence of the latter acid has a significantly better resolution and could be interpreted in full detail. NOE correlations observed between the C*H*Cl_2 signal of the guest DCA anion and resonances of the macrocyle (NH-**b** and *endo*-*o*-Mes-**b**) provided a strong indication of the binding mode (Figure 8). In addition, the location of the anion in the

(26) Becker, E. D.; Bradley, R. B. *J. Chem. Phys.* **1959**, *31*, 1413–1414.
(27) Sondheimer, F. *Acc. Chem. Res.* **1972**, *5*, 81–91.

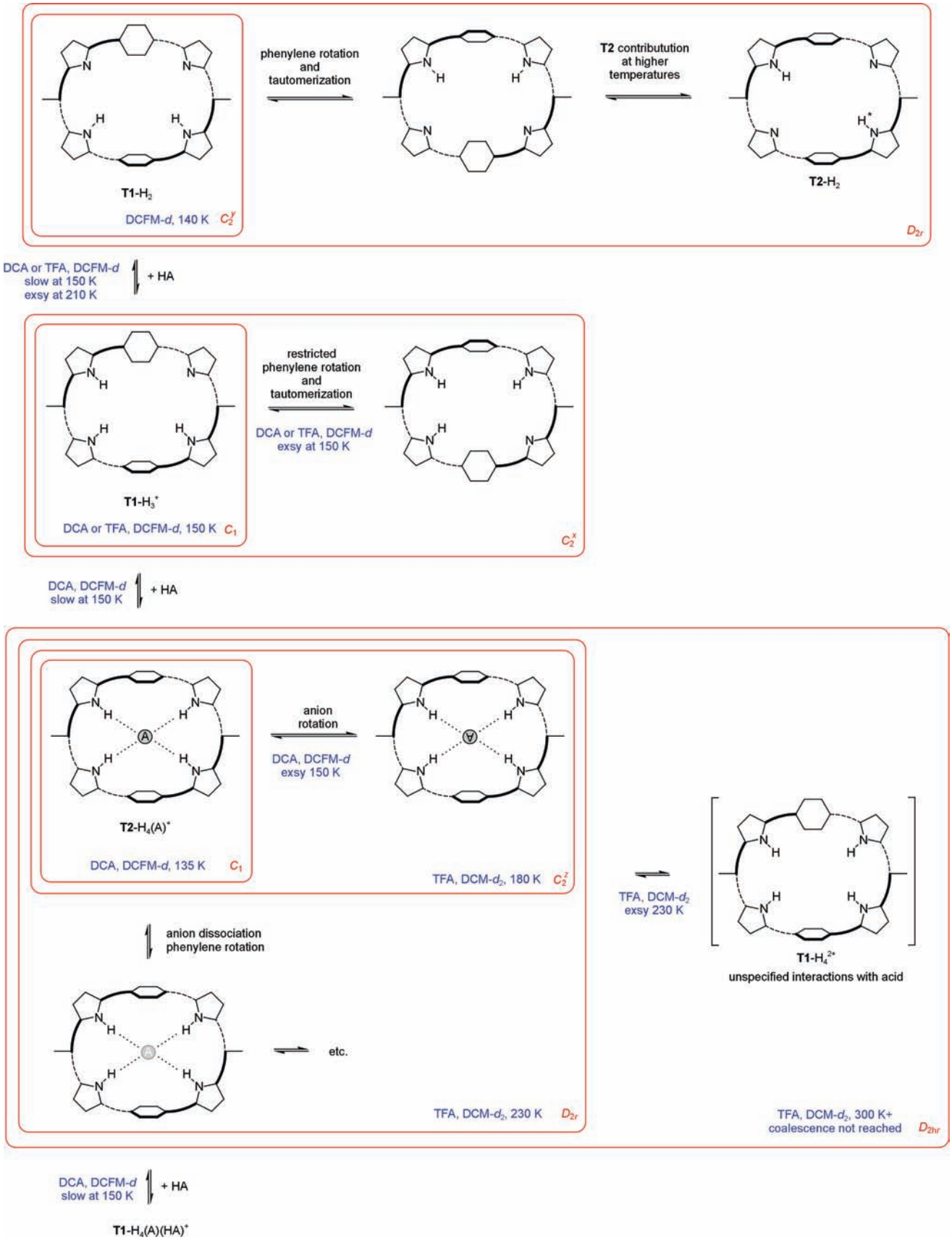

Figure 5. Dynamic processes observed in di-*p*-benzihexaphyrin upon protonation (continued in Figure 10). Effective symmetries, observed directly (in 1D spectra) or indirectly (via EXSY), are indicated in red. Red boxes show which forms and processes contribute to the observed effective symmetry. Specific conditions (acid, solvent, temperature) are shown in blue. A black "A" denotes the anion residing in the front groove and pointing its R group toward the viewer. A white "A" denotes the anion residing in the back groove and pointing the R group away from the viewer. When it is drawn upside down, "A" corresponds to the anion rotated by 180° in the cavity.

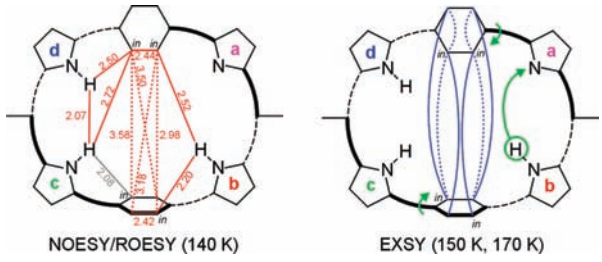

Figure 6. Correlations observed in the ^{1}H NOESY and ROESY spectra of **T1**-H_3^+, used for partial signal assignment (DCFM-*d*, 140−170 K, NOE in red, exchange in blue). Hydrogens attached to carbons are implicit. Weaker correlations are indicated as dotted lines. Some expected cross-peaks could not be identified in the more crowded regions of the 2D spectra (shown in gray). Values in red are interhydrogen distances (Å) taken from a DFT model (KMLYP/6-31G**). The exchange pattern (solid blue lines) corresponds to restricted ~90° rotations of the phenylenes, in the direction indicated by green arrows, coupled with a proton transfer step. The protonation pattern given in the figure (quadrants **b**−**d**) was selected on the basis of the relative cross-peak intensities for the interactions NH-**b**···*in*-phenylene-**b** (stronger) and NH-**b**···*in*-phenylene-**a** (weaker).

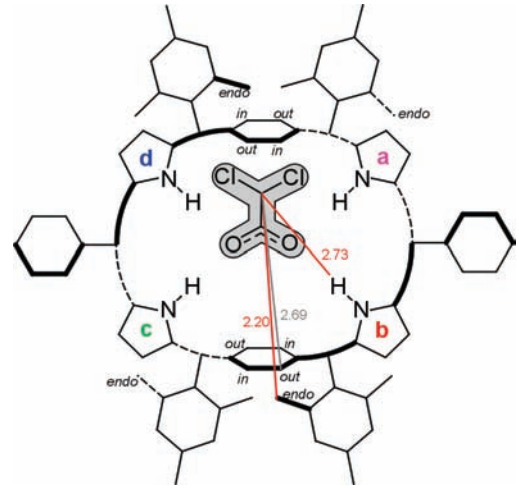

Figure 8. Intermolecular NOE correlations (shown as red lines) observed in the ROESY spectrum of [**T2**-H_4(A)]$^+$ (A = DCA), used for signal assignment (DCFM-*d*, 135 K). Hydrogens attached to carbons are implicit. NOE shown in gray could not be observed because of a small difference of chemical shifts between the corresponding signals (0.31 ppm) and severe crowding in this region. Interhydrogen distances (Å) have been taken from a KMLYP/6-31G** model. For a three-dimensional representation of this structure see Figure 3.

macrocyclic core is consistent with the two-step dynamic behavior observed at higher temperatures (see discussion below). The ^{1}H NMR shifts are satisfactorily reproduced by the GIAO/KMLYP calculation (Figure S12).

Variable-temperature ^{1}H NMR data obtained at 600 MHz provide insight into the dynamics of the host−guest complex [**T2**-H_4(A)]$^+$ (Figures 5 and S7). The R group of the anion (CF_3 or $CHCl_2$) is able to rotate in the groove, and this rotation can only be locked at very low temperatures. At 135 K in DCFM-*d*, both the DCA and TFA complexes display C_1-symmetric spectra of very similar appearance. The particularly well-resolved spectrum of [**T2**-H_4(DCA)]$^+$ was amenable to detailed structural analysis. A broadened C_1-symmetric spectrum can also be observed at 165 K for [**T2**-H_4(TFA)]$^+$ dissolved in DCM-d_2 (Figure S7). As the temperature is increased to ca. 230 K, the spectral pattern goes through two coalescence steps, the first of which results from the fast rotation of the R group, which results in pairwise equivalence of quadrants (**a**−**c** and **b**−**d**). It should be noted that, unlike $CHCl_2$, the CF_3 group has 3-fold symmetry and only a 60° rotation is needed to effect exchange. Alternatively, a dissociative mechanism can be considered, which apparently implies a higher activation barrier but cannot be

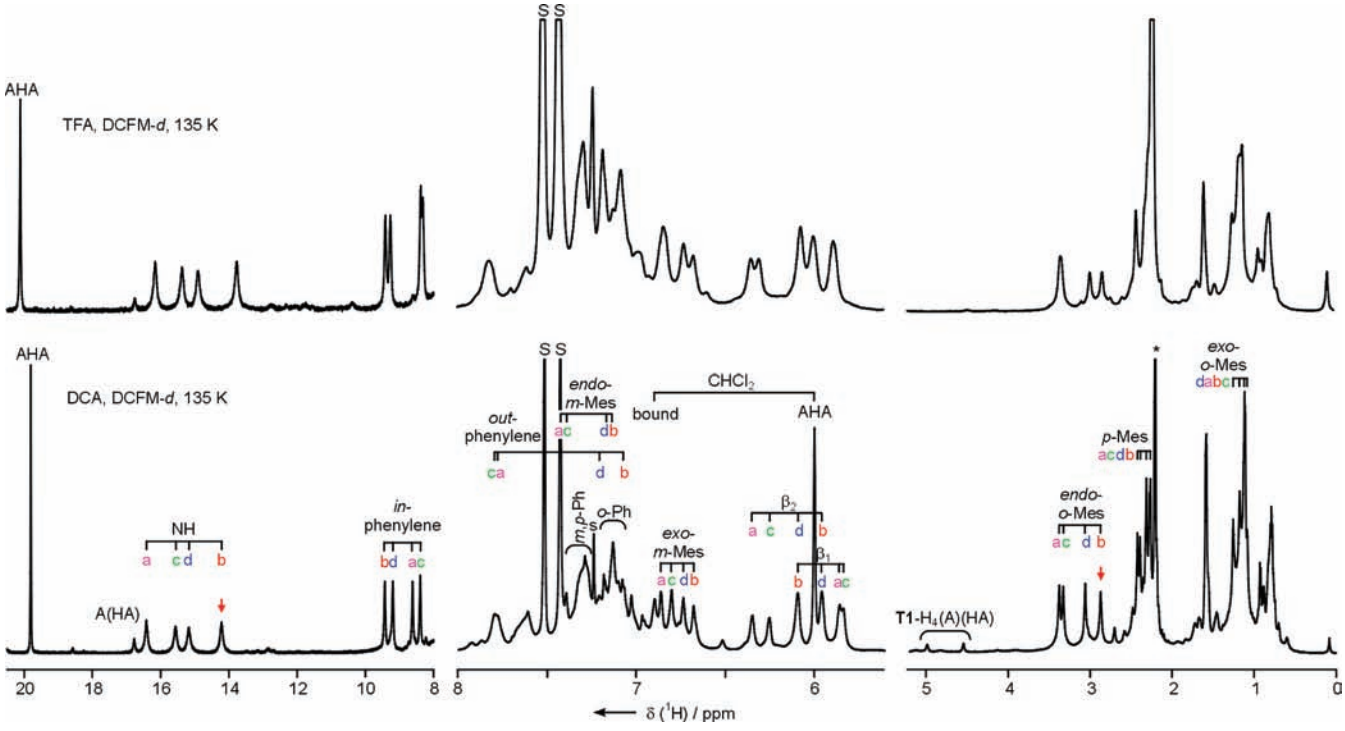

Figure 7. ^{1}H NMR spectra of [**T2**-H_4(A)]$^+$[AHA]$^-$ (600 MHz, DCFM-*d*, 135 K). The top and bottom spectra correspond to A = trifluoroacetate (TFA) and A = dichloroacetate (DCA), respectively. AHA is the hydrogen dicarboxylate anion. In the bottom spectrum, the C*H*Cl_2 proton of the bound DCA yields NOE's with the protons indicated with red arrows. Atom labeling is explained in Figure 4. For related 2D spectra see Figures S26−S32. 1D spectra of the remaining species and corresponding 2D maps can be found in the Supporting Information.

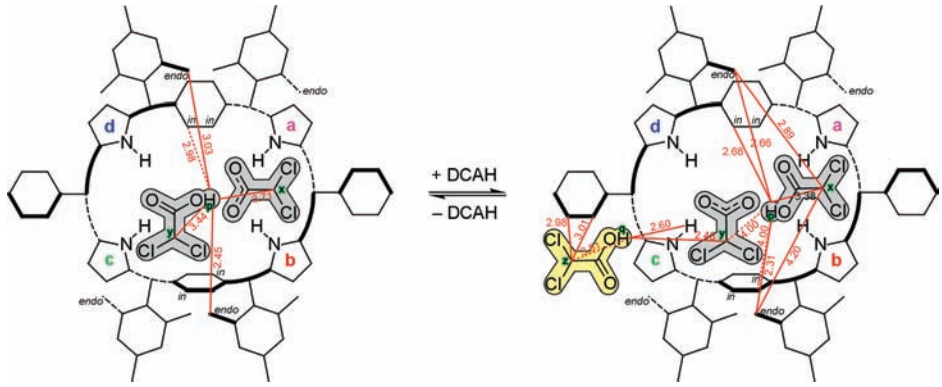

Figure 9. Intermolecular NOE correlations (shown as red lines) observed in the NOESY and ROESY spectra of [**T1**-H_4(A)(HA)]$^+$ and [**T1**-H_4(A)$(HA)_2$]$^+$ (A = DCA), used for signal assignment (DCFM-*d*, 150 K). Hydrogens attached to carbons are implicit. C*H*Cl_2 protons are labeled as *x*, *y*, and *z*, and O*H* protons are labeled as *p* and *q*. Weaker correlations are shown as dotted lines. Association of the additional DCAH molecule (*z*) is reversible and induces the transfer of proton *p* from residue *y* to *x*. Interhydrogen distances (Å) have been taken from a KMLYP/6-31G** model. For three-dimensional representations of these structures see Figure 3.

distinguished from the R group rotation on the basis of available data. According to this mechanism, the anion is temporarily removed form the groove and rotates freely before returning to the cavity. However, the interaction between the macrocycle and the anion must be relatively tight because return takes place in the original groove.

The second step, which leads to a spectrum with 4-fold symmetry, is a consequence of complete dissociation of the anion from the core. In this step, the anion does not form a tight ion pair with the macrocycle and, when the complex is re-formed, either of the two grooves can be filled. Consequently, any of the four equivalent arrangements may be selected, resulting in complete equivalence between the four quadrants. Upon a further increase in temperature, the coalesced spectrum experiences a gradual change of chemical shifts consistent with a transition to a diatropic structure. At room temperature, the NMR and UV−vis spectral parameters give a strong indication that the dication exists predominantly as the Möbius form [**T1**-H_4]$^{2+}$, with a possible small contribution of [**T2**-H_4]$^{2+}$. As discussed below, the Möbius dication is conformationally unstable and has a limited lifetime at room temperature. The extent of acid association to [**T1**-H_4]$^{2+}$, which is of importance at low temperatures, could not be determined on the basis of room-temperature spectra.

[T1-H_4(A)(HA)]$^+$ and [T1-H_4(A)$(HA)_2$]$^+$. As described for [**T2**-H_4(A)]$^+$, NMR spectra obtained in the presence of DCAH had superior resolution and could be used for detailed structural investigation (Figure S3). The first species, [**T1**-H_4(A)(HA)]$^+$, is observed transiently during the titration and is thus always accompanied by other forms. Consequently, only partial assignment of its ^{1}H NMR spectrum was possible, which was achieved by analyzing intermolecular exchange between [**T1**-H_4(A)(HA)]$^+$ and [**T1**-H_4(A)$(HA)_2$]$^+$ (A = DCA), as observed in a NOESY spectrum at 150 K. This strategy was very effective, because a complete assignment was obtained for [**T1**-H_4(A)$(HA)_2$]$^+$, which becomes the dominant species at the end of the titration. Except for the number of $CHCl_2$ signals, the spectral patterns are qualitatively similar for both species and show definite characteristics of a diatropic system. The major difference between the two spectra is the intensity of the macrocyclic ring current, which is more pronounced in [**T1**-H_4(A)$(HA)_2$]$^+$ (see below). The spatial arrangement of coordinated acid relative to the macrocyclic ring was established for [**T1**-H_4(A)(HA)]$^+$ and [**T1**-H_4(A)$(HA)_2$]$^+$ (A = DCA) on the basis of intermolecular NOE contacts observed in 2D NMR spectra at 150 K (Figures 9 and S4). The viability of the resulting structural models was verified with DFT calculations and simulation of NMR shifts (see discussion below).

Acid association to [**T1**-H_4(A)(HA)]$^+$ and [**T1**-H_4(A)$(HA)_2$]$^+$ is reversible and subject to chemical exchange at higher temperatures (Figure 10). At 150 K, [**T1**-H_4(A)(HA)]$^+$ undergoes reorganization of acid units in the groove, which is coupled to restricted rotation of phenylene rings. In contrast, [**T1**-H_4(A)$(HA)_2$]$^+$, investigated at 150 K and at a higher DCAH concentration, only shows exchange between the associated DCAH molecules and the bulk acid. As the additional acid molecule is held in place by only one hydrogen bond, it is observed to exchange more rapidly with the bulk acid than the two acid units originally present in [**T1**-H_4(A)(HA)]$^+$. When the temperature is raised to 170 K, the exchange pattern of [**T1**-H_4(A)$(HA)_2$]$^+$ is consistent with the acid molecules being bound randomly in each of the two grooves of the macrocycle. As this exchange is not connected with phenylene rotation, it is likely that under these conditions exchange of acid proceeds via an associative mechanism.

[T0-H_4]$^{2+}$ and T0-H_2. Complete conversion of di-*p*-benzihexaphyrin to the planar dication [**T0**-H_4]$^{2+}$ is achieved by acidifying a sample with TFAH and leaving it at room temperature for several hours. Directly after addition of acid, the dication exists primarily as the Möbius aromatic conformer [**T1**-H_4]$^{2+}$, which is gradually converted to the planar form (Figure S8). The spectra of [**T0**-H_4]$^{2+}$, recorded at 300 K (DCM-d_2) and 150 K (DCFM-*d*) are shown in Figure S5. At 300 K the phenylene rings are engaged in a rapid flipping motion, which results in the averaging of the *in* and *out* signals (Figure 11). In the slow exchange limit, observable at or below 150 K, the signals are decoalesced and separated by nearly 5 ppm, clearly showing the effect of macrocyclic paratropicity. Depending on the relative orientation of the tilted rings, the macrocycle can adopt several conformations, the most probable of which have point symmetries C_2^z and C_i and will give rise to effectively indistinguishable spectral patterns. The C_i structure is analogous to the solid-state conformation of [**T0**-H_4]$^{2+}$ and is predicted to be minimally more stable than the C_2^z conformer (B3LYP/6-31G**, Table S5). The primary hydrogen-bonding interaction between the macrocycle and the carboxylate anions is via the peripheral NH protons (NH-**b**), leading to a marked dependence of the chemical shift on the anion used. In the case of the weakly

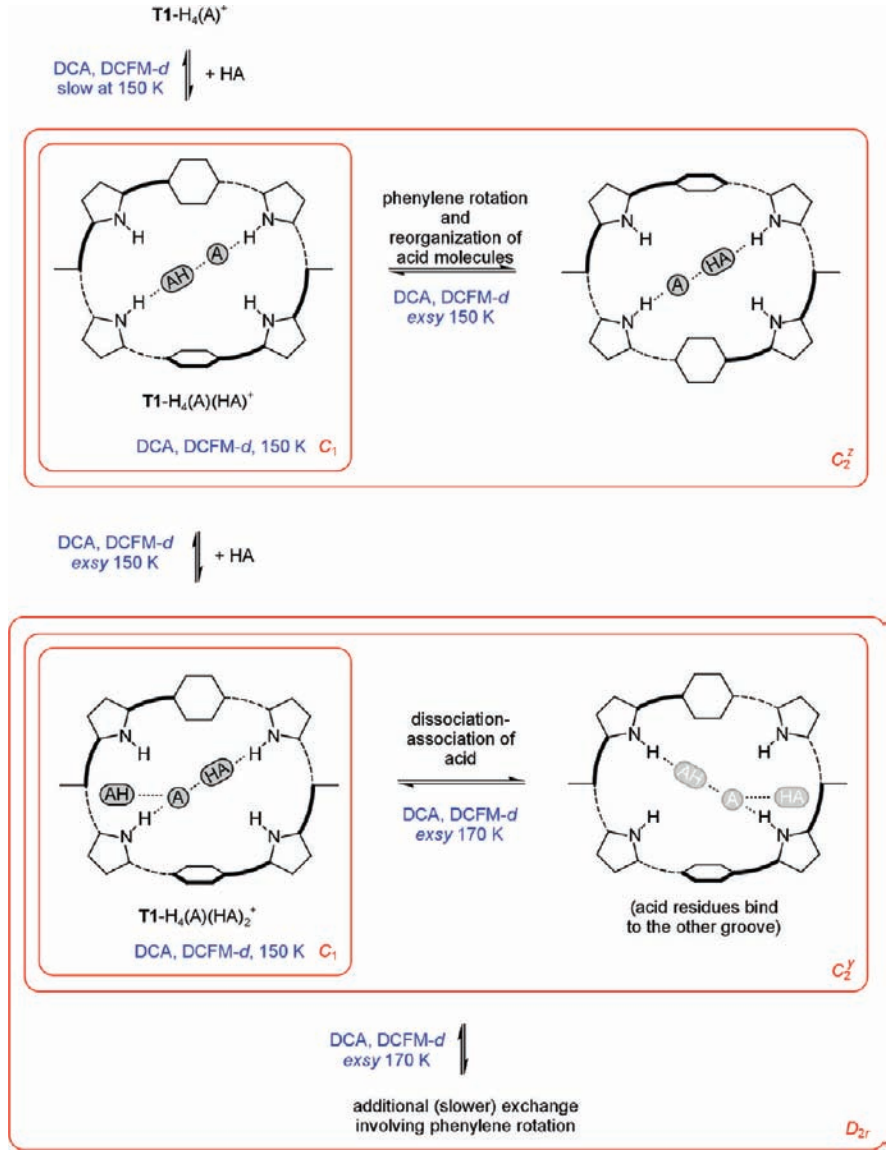

Figure 10. Dynamic processes observed in di-*p*-benzihexaphyrin upon protonation (continued from Figure 5). Effective symmetries, observed directly (in one-dimensional spectra) or indirectly (via EXSY), are indicated in red. Red boxes show which forms and processes contribute to the observed effective symmetry. Specific conditions (acid, solvent, temperature) are shown in blue. White letters denote acid molecules residing in the back groove.

coordinating TFA anion, the shift is 5.30 ppm (DCFM-*d*, 150 K, excess acid), whereas in the presence of DCA, the shift is 6.42 ppm (same conditions). Still, the interaction with the DCA anion is weaker and less specific than those observed for the cationic forms of the twisted **T1** and **T2** conformations.

The principal structural characteristics of [**T0**-H_4]$^{2+}$ are preserved in the solid state. In the crystal, the **T0** dication forms a hydrogen-bonded aggregate, in which two TFA anions interact with the peripheral NH groups of the macrocycle and are accompanied by four TFAH molecules (Figures 3 and S1). A similar conformation, stabilized by intramolecular hydrogen bonding, has recently been reported in a doubly N-confused analogue of di-*p*-benzihexaphyrin.[25]

The planar free base was generated from the dication [**T0**-H_4]$^{2+}$ by low-temperature addition of triethylamine to a DCM-d_2 sample acidified with TFAH. Partial conversion to **T1**-H_2 could not be avoided, due to local overheating of the sample (Figure S5). Once the sample temperature was stabilized at or below 190 K, the concentration of **T0**-H_2 remained constant for several hours, sufficient to perform variable-temperature measurements and record 2D spectra. At 210 K, the rate of folding increases measurably and partial conversion of **T0**-H_2 into the mixture of **T1**-H_2 and **T2**-H_2 is observed over the course of several hours. The protonation pattern of the free base **T0**-H_2 was unambiguously determined using a COSY spectrum. The system exhibits a fast flipping motion of the phenylene rings similar to that observed in [**T0**-H_4]$^{2+}$ (Figure 11). This dynamic process can be frozen out at 160 K, making it possible to identify the outer and inner phenylene signals. In analogy to [**T0**-H_4]$^{2+}$, there are two possible conformers of the free base, which differ in the relative orientations of the phenylene rings. The C_2^z structure has a slightly lower energy (B3LYP/6-31G**, Table S5) and was chosen for the prediction of NMR and electronic spectra.

Electronic Spectroscopy. Topology switching has a marked influence on the electronic spectrum of di-*p*-benzihexaphyrin (Figure 12). Each of the free bases has a distinct spectral pattern with two principal, rather broad absorption maxima in the visible region. The absorption profiles are significantly different for each conformer, producing diverse colors for different twist

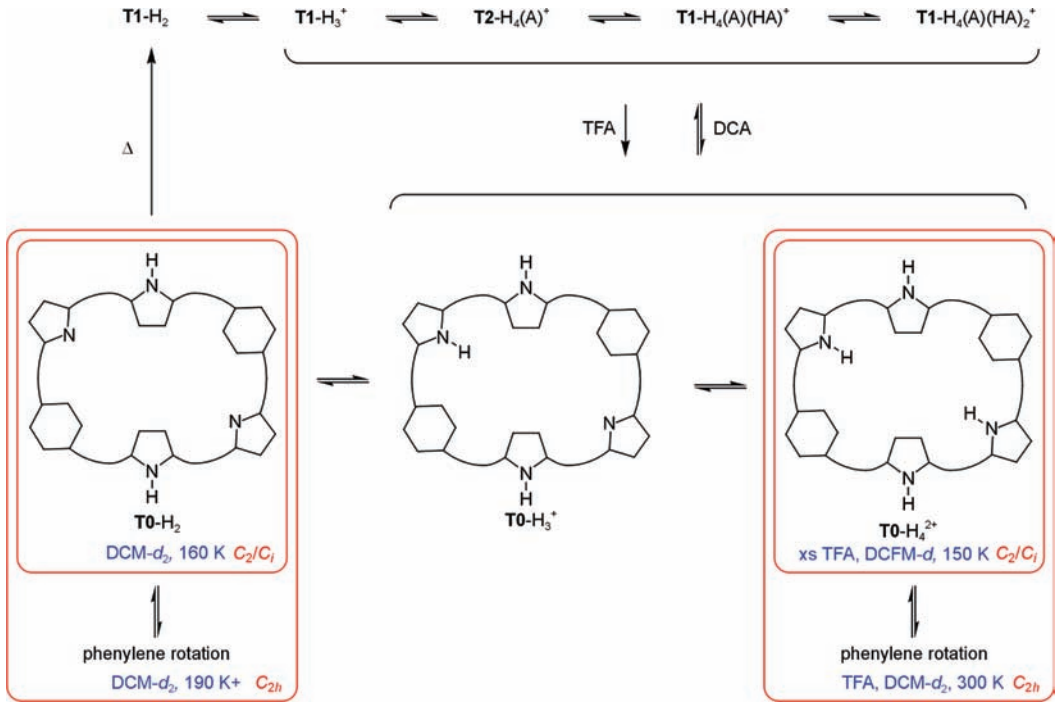

Figure 11. Conversion of hexaphyrin to the **T0** conformer and dynamic processes observed for the **T0** forms. Effective symmetries, observed directly (in one-dimensional spectra) or indirectly (via EXSY), are indicated in red. Red boxes show which forms and processes contribute to the observed effective symmetry. Specific conditions (acid, solvent, temperature) are shown in blue. Note: in the presence of TFAH, the spectrum of [**T0**-H_4]$^{2+}$ in DCFM-*d* becomes more complicated at 135 K. This is likely due to an unspecified interaction with the anion or/and additional conformational equilibrium.

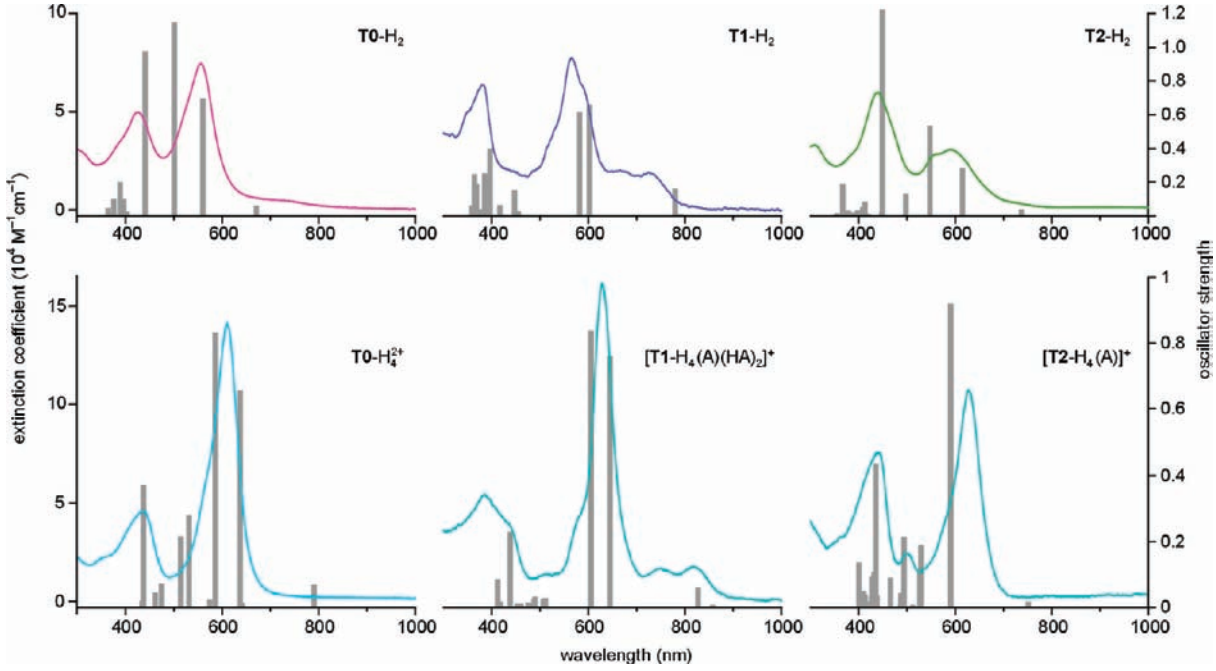

Figure 12. Electronic spectra of free bases **T0**-H_2, **T1**-H_2, and **T2**-H_2 and the corresponding dications. Conditions: **T0**-H_2, DCM, 25 °C (transient spectrum); **T1**-H_2, DCM, −90 °C; **T2**-H_2, hexane, 25 °C; **T0**-H_4^{2+}, DCM, TFAH, room temperature; [**T1**-H_4(A)$(HA)_2$]$^+$, DCM, −90 °C, A = TFA; [**T2**-H_4(A)]$^+$, DCM, −90 °C, A = TFA. Vertical bars denote TD DFT transitions calculated at the B3LYP/6-31G** level of theory (A = DCA for **T1** and **T2** dications).

levels. In contrast, the colors of dications are rather similar shades of blue and are largely determined by one strong absorption band, at ca. 610−630 nm. For each twist level, protonation of the free base induces a red shift of the most intense bands combined with an increase in absorptivity, which is a typical behavior of many porphyrinoids. The Möbius structure **T1**-H_2 is distinguished from the Hückel systems by the presence of two red-shifted bands at 665 and 725 nm, a feature that is preserved in the cationic species [**T1**-H_4(A)$(HA)_2$]$^+$ (bands at 752 and 815 nm). The spectral patterns were correctly reproduced by time-dependent (TD) DFT calculations. However, the TD method predicts only one red-shifted

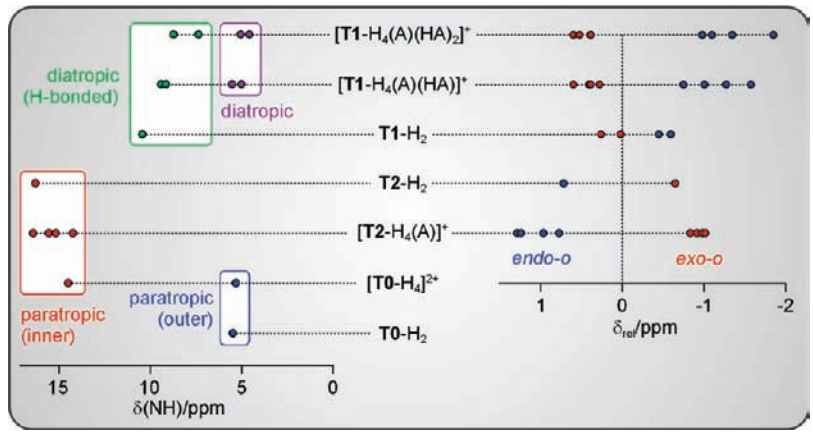

Figure 13. ^{1}H NMR shifts of the NH protons (left) and *o*-Mes protons (right) for selected forms of A,D-di-*p*-benzihexaphyrin (A = DCA). Shifts of the *o*-Mes protons are given relative to the corresponding shift of 5-mesityldipyrrin (2.10 ppm).[38] The definition of endo and exo positions is given in Figure 3. For experimental conditions, see the Supporting Information.

transition in each of the Möbius forms, indicating that the other one may be vibronically allowed, similar to what is observed in a related all-pyrrole hexaphyrin.[11]

Ring Currents and Hydrogen Bonding. While the topology of a π-conjugated system is easily determined by examining torsional angles in the ring, the assessment of Möbius aromaticity on the basis of established criteria (energetic, structural, or magnetic) is more challenging, occasionally creating controversy.[3,28] The difficulty can in part be ascribed to the scarcity of Möbius aromatics and to their unique structural and electronic properties. In order to accommodate a 180° twist, the ring has to be relatively large, and the smallest Möbius aromatic ring isolated to date contained an [16]annulenoid pathway.[2,3] The unfavorable consequence of large molecular sizes is the difficulty in obtaining reliable geometries (both experimental and calculated), which are necessary not only for evaluation of structural aromaticity indexes[29] but also for accurate prediction of chemical shifts.[30] Furthermore, the structural and magnetic effects of aromaticity and antiaromaticity tend to be less pronounced in Möbius systems because of their size and nonplanarity.[2,6,7] Nevertheless, in the case of porphyrin analogues, ^{1}H NMR chemical shifts remain the most convenient experimental measure of aromatic character[31] and were proved to be equally applicable to porphyrinoid Möbius systems.[6−11] A useful feature of many porphyrinoid derivatives is the availability of protons located inside the macrocyclic ring, which is strongly affected by ring currents and can serve as a sensitive aromaticity probe. In the present case, macrocyclic ring currents noticeably affect the shielding of *in*-phenylene and NH protons (Table S4). In particular, the *in*-phenylene shifts range from 2.95 ppm in the diatropic [**T1**-H_4(A)$(HA)_2]^+$ (A = DCA) to 11.25 ppm in [**T0**-$H_4]^{2+}$. The chemical shifts of NH protons are influenced not only by ring currents but also by hydrogen bonding, offering additional insight into the structure of adducts (Figure 13, left). These hydrogen bonds, which consistently provide a downfield contribution to the observed shifts, are either intramolecular NH···N interactions present in the free bases **T1**-H_2 and **T2**-H_2 or intermolecular NH···O contacts involving carboxylic groups. Intramolecular NH···N hydrogen bonds of varying strength have been observed in a number of porphyrin analogues, representative examples including porphycene,[32,33] isocorrole,[34,35] N-fused porphyrin,[36] and subpyriporphyrin.[37] Deshielding of two "opposite" NH protons in the Möbius adducts [**T1**-H_4(A)(HA)]$^+$ and [**T1**-H_4(A)$(HA)_2]^+$ is consistent with binding of all acid residues in one groove. The chemical shifts of inner NH protons are in the same range for the two paratropic species [**T2**-H_4(A)]$^+$ and [**T0**-$H_4]^{2+}$, but they cannot be directly compared. In the latter species, the quasi-planar geometry results in a more effective paratropic deshielding of the inner NH; however, this difference is more than compensated by the hydrogen bonding present in [**T2**-H_4(A)]$^+$. As evidenced by experimental and computational data, hydrogen bonding also affects the NH shifts of [**T1**-$H_3]^+$ and [**T0**-$H_4]^{2+}$ (peripheral NH groups), but the effect is weaker and only becomes relevant in the presence of DCA anions. In DCA adducts with folded conformations (**T1** or **T2**), the $CHCl_2$ groups of associated acid molecules are exposed to the ring current effects of the macrocycle, providing an "external" aromaticity probe. The chemical shift of the C*H*Cl_2 proton in DCAH itself is relatively insensitive to the protonation state, and it resonates at 6.00 ppm in the hydrogen bis(dichloroacetate) anion (DCFM-*d*, 150 K). In [**T1**-$H_4]^{2+}$ adducts, the C*H*Cl_2 protons are shielded by the diatropic ring current, the lowest recorded shielding being 4.52 ppm. Conversely, the C*H*Cl_2 signal in [**T2**-H_4(DCA)]$^{2+}$ is shifted downfield to 6.90 ppm.

In the case of figure-eight conformations **T1** and **T2** the relative strengths of dia- and paratropic ring currents can be

(28) Castro, C.; Chen, Z.; Wannere, C. S.; Jiao, H.; Karney, W. L.; Mauksch, M.; Puchta, R.; Hommes, N. J.; Schleyer, P. *J. Am. Chem. Soc.* **2005**, *127*, 2425–2432.
(29) Krygowski, T. M.; Cyrański, M. K. *Chem. Rev.* **2001**, *101*, 1385.
(30) Wannere, C. S.; Sattelmeyer, K. W.; Schaefer, H. F.; Schleyer, P. v. *Angew. Chem., Int. Ed.* **2004**, *43*, 4200–4206.
(31) Stępień, M. ; Latos-Grażyński, L. , Aromaticity and Tautomerism in Porphyrins and Porphyrinoids. In *Topics in Heterocyclic Chemistry*; Krygowski, T. M., Cyrański, M. K., Eds.; Springer: New York, 2009; Vol. 19, pp 83−153.
(32) Vogel, E.; Köcher, M.; Lex, J.; Ermer, O. *Isr. J. Chem.* **1989**, *29*, 257–266.
(33) Waluk, J. *Acc. Chem. Res.* **2006**, *39*, 945–952.
(34) Will, S.; Rahbar, A.; Schmickler, H.; Lex, J.; Vogel, E. *Angew. Chem., Int. Ed. Engl.* **1990**, *29*, 1390–1393.
(35) Vogel, E.; Binsack, B.; Hellwig, Y.; Erben, C.; Heger, A.; Lex, J.; Wu, Y.-D. *Angew. Chem., Int. Ed. Engl.* **1997**, *36*, 2612–2615.
(36) Furuta, H.; Ishizuka, T.; Osuka, A.; Ogawa, T. *J. Am. Chem. Soc.* **1999**, *121*, 2945–2946.
(37) Myśliborski, R.; Latos-Grażyński, L.; Szterenberg, L.; Lis, T. *Angew. Chem., Int. Ed.* **2006**, *45*, 3670–3674.
(38) Yu, L.; Muthukumaran, K.; Sazanovich, I. V.; Kirmaier, C.; Hindin, E.; Diers, J. R.; Boyle, P. D.; Bocian, D. F.; Holten, D.; Lindsey, J. S. *Inorg. Chem.* **2003**, *42*, 6629–6647.

demonstrated by comparing the chemical shifts of *o*-methyl groups located on the mesityl substituents (Figure 13, right). The figure-eight fold of the macrocycle places the two *o*-methyl groups of each substituent in different zones of the shielding cone, resulting in a significant differentiation of their chemical shifts. In the case of diatropic **T1** structures, the *endo* protons (located closer to the groove, Figure 3, top right) are shielded by up to 2 ppm relative to the reference shift of 5-mesityldipyrrin,[38] whereas the *exo* protons experience a smaller deshielding effect. In the **T2** conformations, the shifts of the *endo* and *exo* protons are reversed, confirming the switching to a paratropic structure. The ring currents, both dia- and paratropic, are noticeably enhanced by protonation. In the case of **T0** conformations, shielding of all *o*-mesityl groups is consistent with the paratropic character of a planar Hückel structure. The ring currents were also demonstrated computationally by evaluating nucleus-independent chemical shifts (NICS)[39] for structures representing the three twist levels (Table S6). Systems containing Hückel-type π-surfaces (**T0** and **T2**) consistently yielded positive NICS values for points contained inside the macrocycle. In contrast, shifts calculated for Möbius structures were uniformly negative.

To further test the integrity of the assignment and the validity of the DFT models, proton chemical shifts were calculated at the GIAO/KMLYP/6-31G** level of theory (see the Supporting Information). For the free bases **T0**-H_2, **T1**-H_2, and **T2**-H_2, the experimental values were reproduced remarkably well, indicating that the DFT calculations accurately model not only the conformations of the hexaphyrin ring but also the extent of π-conjugation.[30] The agreement between calculated and experimental shifts is also very good for $[\mathbf{T0}\text{-}H_4]^{2+}$ and $[\mathbf{T2}\text{-}H_4(A)]^{+}$; it is however less satisfactory, albeit still acceptable, in the case of $[\mathbf{T1}\text{-}H_4(A)(HA)_2]^{+}$ (A = DCA). In the latter adduct, the conformation of the macrocycle, which directly affects the ring current, is dependent on hydrogen-bonded interactions with three acid molecules, which are more loosely bound than the anion in $[\mathbf{T2}\text{-}H_4(A)]^{+}$. As a consequence, relatively small variations in the equilibrium geometry of the hydrogen bonds, which are known to result from solvation,[40] may be translated into significant changes of chemical shifts.

Energetics. The multilevel topology switching observed in di-*p*-benzihexaphyrin, like any observable conformational equilibrium, requires that the conformers involved have comparable energies and are separated by thermally accessible transition states. Relative gas-phase energies (B3LYP/6-31G**) calculated for the most stable tautomers of **T0**-H_2, **T1**-H_2, and **T2**-H_2 are 8.99, 2.22, and 0.00 kcal/mol, respectively. The highest value obtained for **T0**-H_2 corresponds to the observed metastability of this species. While the energy difference between **T1**-H_2 and **T2**-H_2 is very small, the predicted stability ordering is different from that observed experimentally. As discussed earlier, the Möbius form was found to be the most stable species in DCFM-*d* and pentane-d_{12} solutions at low temperatures and was also characterized in the solid state[6] (to date, we have not been successful in crystallizing the **T2**-H_2 form). This discrepancy may be a result of solvation effects not accounted for in the DFT calculations or may indicate a non-negligible contribution of CH$\cdots\pi$ interactions in **T1**-H_2, which are known to be poorly reproduced by conventional DFT methods.[41] In contrast to the case for the free base, $[\mathbf{T0}\text{-}H_4]^{2+}$ is predicted to be the preferred dicationic species in the absence of counteranions. This result provides a rationale for the spontaneous planarization process. The other two conformers, $[\mathbf{T1}\text{-}H_4]^{2+}$ and $[\mathbf{T2}\text{-}H_4]^{2+}$, have relative energies of 3.28 and 6.42 kcal/mol, respectively, suggesting that under appropriate experimental conditions they might coexist with the planar $[\mathbf{T0}\text{-}H_4]^{2+}$. Indeed, the three topologies of the dication, **T0**-H_4^{2+}, **T1**-H_4^{2+}, and **T2**-H_4^{2+}, are in a slowly settling equilibrium that shows a marked dependence on the type and amount of acid used and is strongly affected by the temperature. At 300 K, the planar **T0**-H_4^{2+} is the dominant form in DCM solutions, and no other species are observed by NMR, even in the presence of a large excess of acid. In the low-temperature limit, as observed in DCFM-*d*, the equilibrium depends on the acid used. In the case of DCAH, **T0**-H_4^{2+} undergoes partial folding when the sample is placed in the NMR spectrometer probe precooled to 150 K. The distribution of folded species forming upon cooling corresponds to the amount of acid present in the sample, with $[\mathbf{T1}\text{-}H_4(A)(HA)_2]^{2+}$ becoming the major folded species at higher acid concentrations. The extent of low-temperature folding is minimized by using TFAH instead of DCAH, which enables qualitative realization of the switching cycle depicted in Figure 2A.

Conclusions

The example of di-*p*-benzihexaphyrin demonstrates that an appropriately engineered π-conjugated surface may switch between several topologically distinct states in a controllable manner. The crucial part of such engineering involves finding a macrocyclic system that is large and flexible enough to accommodate different levels of twist without excessive strain but has a sufficiently small number of degrees of freedom to keep the conformational processes under control. Fine adjustment of these features seems to be possible in medium-sized expanded porphyrins; as these are responsive to a variety of physical and chemical stimuli, they may ultimately yield topological switches of practical value.

Acknowledgment. The work was supported by the Ministry of Science and Higher Education (Grant No. N204 013536). Quantum chemical calculations were performed in the Wrocław Center for Networking and Supercomputing. We thank Prof. Tadeusz Lis and Dr. Andrzej Bil (University of Wrocław) for their assistance and discussions.

Supporting Information Available: Text, tables, figures, and a CIF file giving materials and methods, additional structural views, NMR spectra, X-ray structural data, and DFT-optimized Cartesian coordinates. This material is available free of charge via the Internet at http://pubs.acs.org.

JA909913Y

(39) Schleyer, P. v. R.; Meaerker, C.; Dransfeld, A.; Jiao, H.; Hommes, N. J. *J. Am. Chem. Soc.* **1996**, *118*, 6317.
(40) Shenderovich, I. G.; Burtsev, A. P.; Denisov, G. S.; Golubev, N. S.; Limbach, H.-H. *Magn. Reson. Chem.* **2001**, *39*, S91–S99.
(41) Lee, E. C.; Kim, D.; Jurecka, P.; Tarakeshwar, P.; Hobza, P.; Kim, K. S. *J. Phys. Chem. A* **2007**, *111*, 3446–3457.